TREE SPECIES CLASSIFICATION FROM AERIAL IMAGES AND LIDAR IN AGRICULTURAL AREAS

Antonio Ruiz[1], Oriol Viñas[1], Albert Domingo[2] and Valentí Marco[2]
[1] Institut Cartogràfic de Catalunya
[2] Departament d'Agricultura, Alimentació i Acció Rural

We present the results of a test study on tree species classification in an agricultural area from digital aerial images and lidar. The objective was to distinguish between three species that are farmed in the area (olive tree, almond tree and carob tree) in order to obtain an efficient technique for reviewing and updating the LPIS (Land Parcel Information System) established by Council regulation (EC) 1782/2003 to check area-based subsidies on agriculture; other species that are present were not considered. Digital aerial photographs with 25 cm pixel were taken with a DMC camera in winter and in summer. Lidar data was acquired with an Optech ALTM 3025 in winter and the point density was 1 point/m^2. Individual trees were detected from lidar data using the hydrographical method. Crown area, tree height, lidar intensity and other parameters describing the structure of the trees were derived from lidar data and for each parameter a raster image was created assigning the same parameter value to every pixel in the crown of each detected tree. These images derived from lidar together with the 4 channel images (R, G, B and IR) from both two epochs were the input for a series of object classification tests done with eCognition image analysis software. In all the tests the object segmentation was based on the tree heights image derived from lidar. A special DSM model including trees was employed in the orthorectification of the DMC images. The best classification results have been obtained using only the orthorectified DMC images at a reduced resolution of 1 m after the tree segmentation from lidar data. Acceptable results have also been obtained from lidar data only.

Introduction

In order to check area-based subsidies on agriculture, the Agriculture Department of our autonomous region asked us to study an efficient technique for reviewing and updating the LPIS (Land Parcel Information System) established by Council regulation (EC) 1782/2003. Most specifically, our goal was to find a method to distinguish and mapping three tree species: olive, almond and carob using remote sensing techniques because the conventional inventory is time consuming and expensive (Viau, 2005). It is common that different species appear mixed in the same stand following different patterns, but only these three species were of interest in this study.

The study area (figure 1) is located south-west of Vila-rodona *(60 km SW of Barcelona)* and has an extension of 6 km x 6 km. It is a dry Mediterranean region where most important crops are vineyards, olive trees, carob trees and almond trees.

Figure 1. Location of study area

Data

Multitemporal digital image data were acquired over the study area with the Cessna Caravan plane of the Institut Cartogràfic de Catalunya (ICC). Two kinds of sensors were installed: the Digital Mapping Camera (DMC) from Intergraph to record spectral data, and the lidar ALTM 3025 from Optech to obtain structural data. All the flights were performed during 2007.

The project area was covered with the DMC on January 17th and on July 19th from 1500 m above ground level, resulting in 70 virtual images for each epoch. This corresponds to a pixel size of 15 cm of the panchromatic channel and to 72 cm of the four low-resolution spectral channels: red, green, blue and near infrared.

From DMC data two kinds of images were created (Figure 2) combining 3 of the 4 colour channels generating the true colour file (channels Blue, Green and Red) and the IRC colour file (channels Green, Red and Infrared)

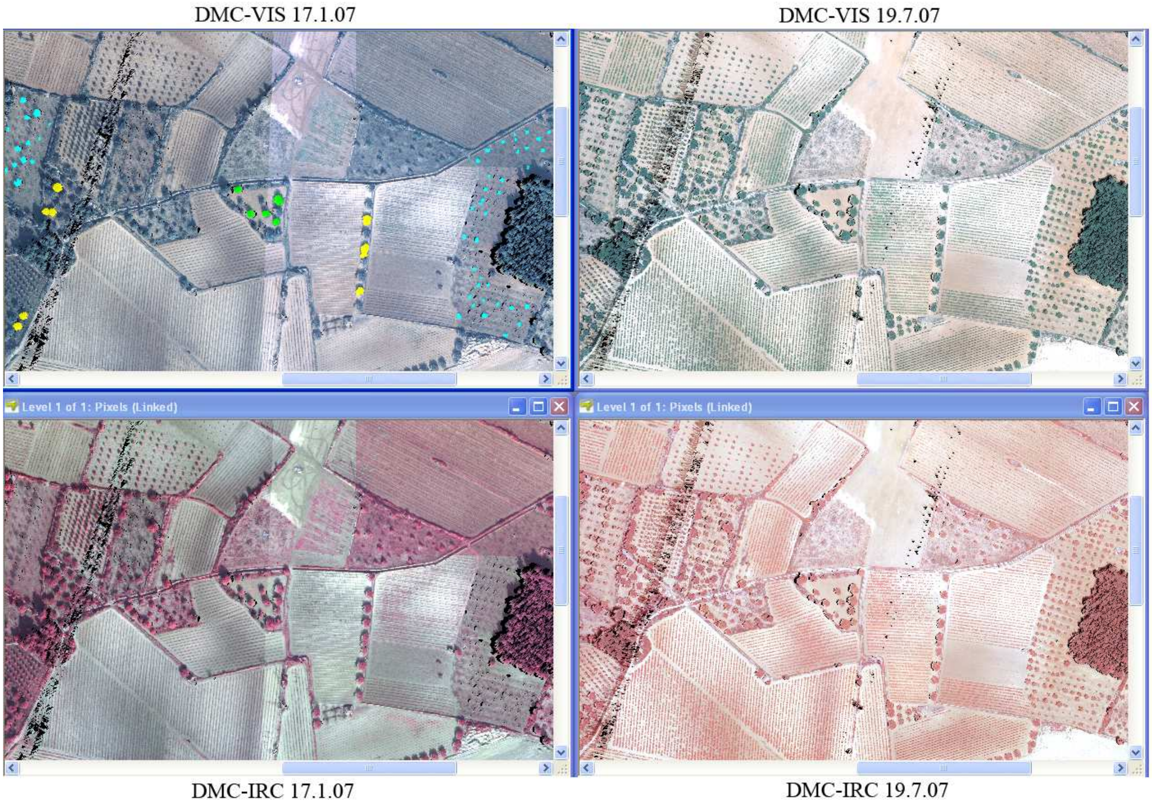

Figure 2. True colour (VIS) images on top and IRC images on bottom. Winter images on the left and summer images on the right. On top left image also the training trees are shown: almond trees in blue, carob in green and olive in yellow. .

After aerial triangulation, DMC images were resampled to 0.25, 0.5 and 1 m pixel sizes using bicubic convolution (Figure 3).

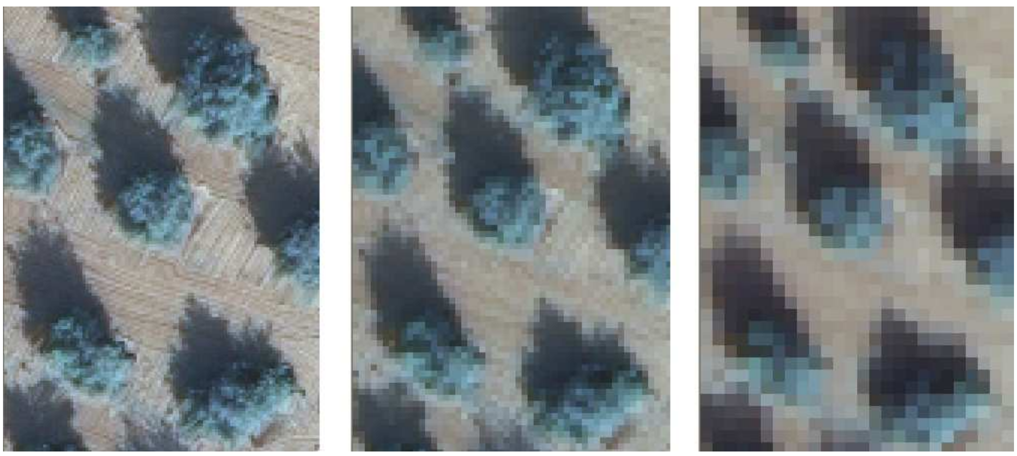

Figure 3. Detail of the images with pixel sizes of 0.25, 0.5 and 1 m from left to right.

At the first stages of the joint processing of DMC images and lidar data, it was noticed that the traditional orthorectification of the images based on a bare-earth DTM was not accurate enough (Palà et al. 2001, Palà & Arbiol, 2002). As the height of the trees had not been taken into account, the crowns appeared shifted and there was a mismatch with the canopy height model (CHM) and between images from different epochs (Lee et al., 2006). The problem was solved rectifying the images with a DSM including tree models where each tree was represented as a generalized cylinder *(see details further on).* The resulting image is not beautiful because black areas appear next to each tree corresponding to the area occluded by the tree but the agreement of the images with the CHM and between them is better (figure 4).

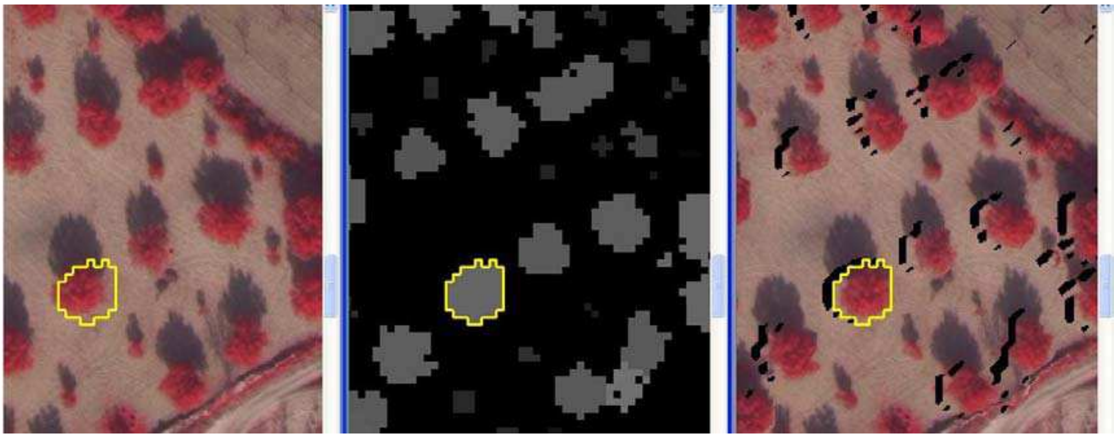

Figure 4. From left to right, orthoimage obtained with DTM, CHM and orthoimage obtained with DSM, and boundary of one of the trees shown in yellow.

Point density	1 point /m^2
Point repetition rate	25000 Hz
Number of strips	24
Scan angle	±11º
Swath	581 m
Strip overlap	50%
Altitude (agl)	1495 m
Speed	130 knots
Footprint	22 cm

Table 1 Lidar parameters.

The area was covered with 24 lidar strips obtained along two flight sessions, on January 17th and 19th. For each single strip, the point density was 0.5 points/m^2 but, as the strip overlap was of 50%, the total point density was 1 point/m^2. Parallel project strips were crossed with two transversal strips over control fields. On each of them, 40 points were measured with GPS/RTK with an accuracy of 2 or 3 cm.

A least squares adjustment was performed to get an elevation offset for each lidar strip following the procedure described in (Kornus & Ruiz, 2003). The observations that entered into the adjustment were the differences between lidar ground points in crossing areas and between strips and control fields. There were a total of 24 strips, 2 control fields plus 3 test areas with different vegetal coverage. The corrections applied to the strips were elevation offsets that ranged from 6.2 to 19.9 cm, all of them positive (upwards). After this correction of systematic errors, lidar points were classified into ground and non-ground points with TerraScan and TerraModeler from Terrasolid. No manual editing was performed after the automatic classification. The accuracy of the resulting terrain model was checked with points measured with GPS/RTK in 3 tests areas with different coverage. The elevation of the points was compared to the elevation of a TIN model built from lidar points classified as ground (bare-earth TIN model). The results of the checking with ground truth are shown in Table 2:

	Area 1	**Area 2**	**Area 3**	**Total**
Coverage	Olive trees	Vinyard	Tennis court	
Approx. vegetation height (m)	1	0.5	0	
# points	20	20	19	59
σ (cm)	5.4	4.5	3.2	4.7
RMS (cm)	6.8	9.3	5.5	7.4
Average Δz (cm)	4.3	8.2	4.6	5.7

Table 2. Checking of bare-earth TIN model with ground truth in 3 test areas.

A digital terrain model (DTM) with 1 m grid step was computed by interpolation on the bare-earth TIN model and a digital surface model (DSM) was computed from all the lidar points taking for each grid cell the elevation of the highest interior lidar point. From the difference between the DSM and DTM a canopy height model (CHM) was computed that was used to detect individual trees with the "hydrological" method. It receives this name because standard GIS tools for hydrological analysis are employed to detect trees (Hyyppä & Inkinen, 1999); in our case, Arc/Info Workstation. The CHM was smoothed with a binomial 3x3 low pass filter and the sign of the heights was changed. Each tree corresponded then to a minimum in the reversed CHM. Each local minimum (sink) corresponds to one individual tree, its depth is the tree height and the area that drains to each sink corresponds to its crown. Most of the trees in this area are isolated and it was considered that each crown finishes when the height reached one third of the total tree height. In this way it was possible to generate one image where all the pixels inside the crown of one tree had the same value corresponding to the height of that tree. In this model each tree is represented as a generalized cylinder. Each tree received a unique identifier and one image of tree identifiers was also generated. In most of the cases, the automatically detected trees correspond to real trees, but sometimes the crown of one tree has split them up into two and they had been considered two different trees by the automatic procedure. In all of the tests, the image segmentation was performed using an image derived from the CHM. We got this image where tree heights are coded in one-byte pixels measuring the height in 20 cm units, i.e. one grey level corresponds to 20 cm.

Using the image of tree identifiers, the corresponding tree identifier was assigned to each lidar point and, after sorting points by tree identifier, a collection of tree parameters was computed. Some of them are an attempt to catch the structural information of the individual trees. The following parameters were computed tree-wise: location coordinates, tree height, crown area, number of points and penetration index. The location was computed as the average of the lidar point coordinates. The penetration index is the ratio between the number of points that reached the ground and the total number of points. From the elevation of the points, it were computed the minimum and maximum, the mean, the standard deviation, the coefficient of variation and the relative height percentiles (5, 10, 15, 20, 25, 30, 50, 75 and 90) (Holmgren, 2003). The coefficient of variation is the ratio between the standard deviation and the mean of a variable. If N is the number of points in the area of one tree crown, the height h of the p-percentile is defined as the elevation above ground of a horizontal plane such that p*N/100 of the points belonging to this tree lay below this plane. If H is the height of the tree, h/H is the relative height of the percentile. From the lidar intensity, the mean, the standard deviation and the coefficient of variation were computed. A raster image was created for each parameter assigning, to every pixel in the crown area, the corresponding value to each tree (Figure 5).

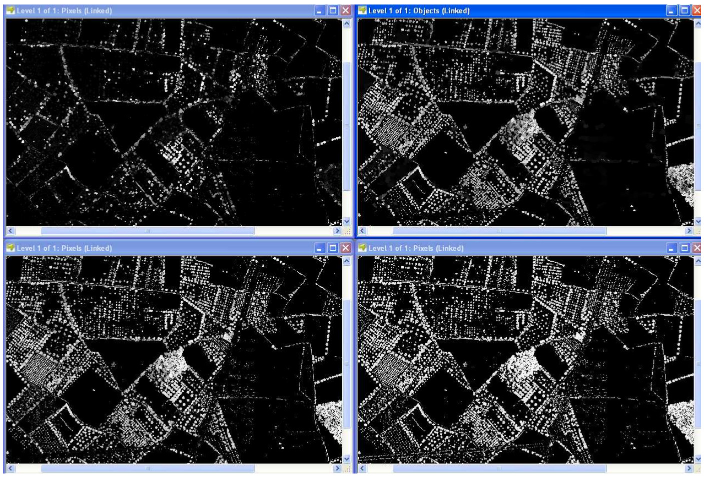

Figure 5. From top to bottom and from left to right: 10, 35, 50 and 90-percentiles of the same area.

Along January 38 trees belonging to the species of interest (Figure 6) were measured. For each tree it was recorded the specie, the location coordinates, the top and bottom height of the crown, the minimum and maximum crown diameters and its pruning and health state. Stands with mixed species are common in the area but there are also homogeneous stands. As a larger training set was required, the boundaries of 31 homogeneous stands were recognized (Figure 6) and in this way it was possible to add more than 300 trees to the 38 field measured data set. Finally, this collection of trees was divided into two independent sets: one to be used as the training set and the other to be used as a test set to analyze the performance of the method.

Field samples concentrate on a small region and the classification testing was restricted to a rectangular area containing the field samples, with UTM-31N coordinates 358658-360456 easting and 4571900-4573000 northing.

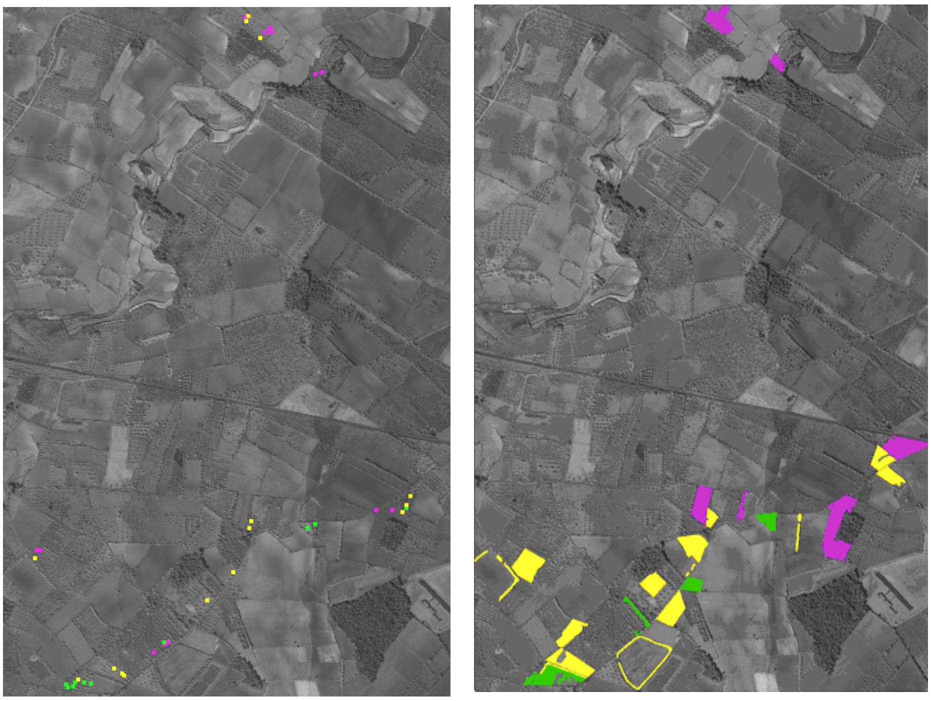

Fig. 6 Left, 38 field measured trees. Right: 31 stands with homogeneous crops.
Olive trees, yellow; carob, green and almond, purple.

Comparison of lidar derived and field measured parameters

A comparison of field measured trees with lidar derived parameters was done. Trees were identified in the CHM image after their coordinates. Field measured tree heights were compared with lidar heights directly. Figure 7a shows that lidar derived heights are in good agreement with field-measured values but dispersion is higher for almond trees. This is a deciduous tree and, at the time of the lidar data capture, they had no leaves. Despite that, almonds were detected with lidar data only.

Crown area was not directly measured on the field but we can estimate it assuming that the shape of the crown projected on the ground is an ellipsis and the maximum and minimum crown diameters are the major and minor axis. Agreement is worse for almond trees. Lidar has a tendency to overestimate the crown area for olive and carob trees (Figure 7b).

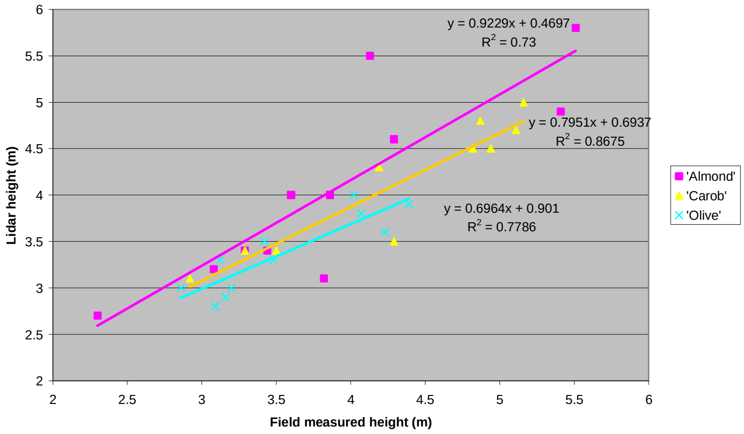

Figure 7a. Tree height regression.

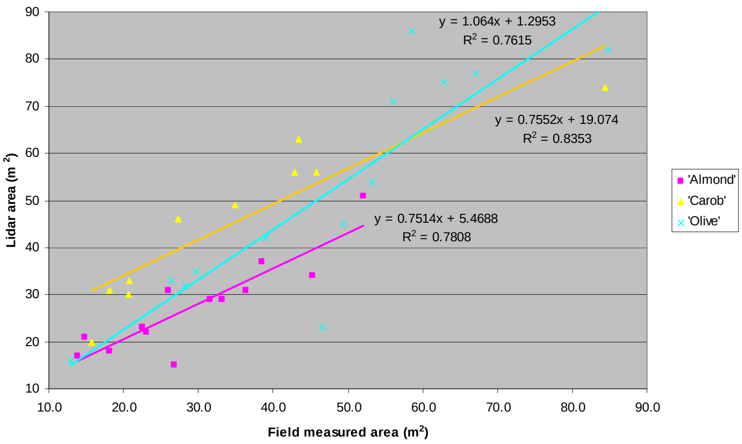

Figure 7b. Crown area regression.

Olive trees and almond trees show a slightly larger area from lidar data that the real value. Tree height was overestimated in 14 cases and underestimated in 19. The crown area was overestimated in 21 cases and underestimated in 14. What we expected was the tree height to be underestimated (Popescu et al., 2004, Næsset & Bjerknes, 2001) because the lidar sampling density was smaller than the lidar footprint and it would be difficult to reach by chance the treetop with the lidar beam. On the opposite, we expected the lidar to overestimate the crown area due to the lidar footprint size.

Methodology

A fundamental problem to apply high resolution digital imagery to this kind of studies is that tree crowns are composed of discrete pixels covering a range of spectral values. Object-based image analysis techniques as opposed to pixel-based software, can be one solution (Chubey, 2006). In our study, image objects corresponding to crowns were singled out with eCognition (Definiens Imaging, 2004). This software provides a processing environment for image analysis whose main characteristic is that the analysis and classification is performed not on individual pixels but on previously generated groups of neighbouring pixels called objects or segments. In a fist step, named multiresolution segmentation, the image is divided into homogeneous regions based on a subset of variables selected by the user and on several user-defined parameters affecting the size, spectral and spatial homogeneity, and shape of the resulting image objects. Once segmented the image, it is possible to start the classification of these segments based on a set of variables selected by the user, using membership functions or maximum likelihood estimation.

Table 3. Segmentation parameters

Pixel size (cm)	Scale	Shape factor	Compactness
25	20	0.3	0.3
50	10	0.3	0.3
100	10	0.3	0.3

After some testing, the idea of individualizing the crowns as segments was accomplished using the tree heigh derived from lidar as the only variable in the segmentation process together with the parameters indicated in Table 3. With these settings, most of the tree crowns were identified as one segment independently of its area (Figure 9).

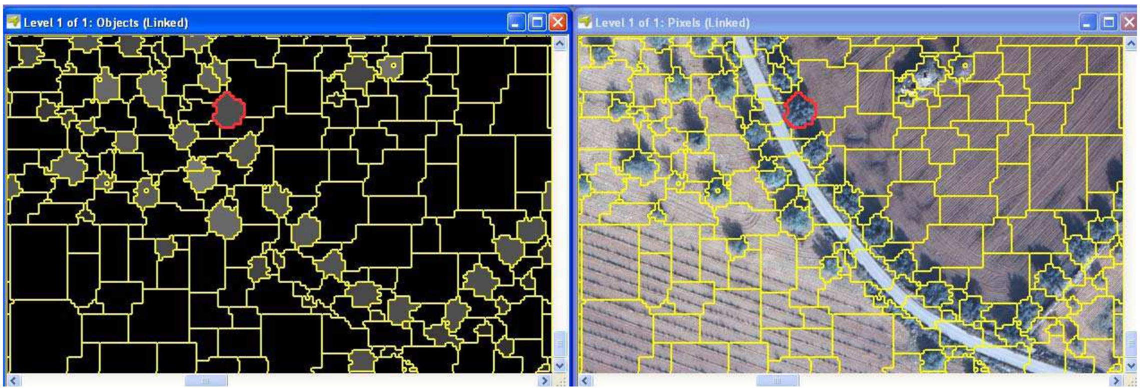

Figure 9. On the left: segmentation results based on the vegetation heigh. On the right: segments boundaries on the DMC image corresponding to the same area.

A series of eCognition trials with different selections of variables was carried out to perform an exhaustive analysis of the available data. There were 27 different trials with different combinations of DMC data: with winter data only, with summer data only and multitemporal. Each of these groups was analyzed at different pixel sizes: 0.25, 05 and 1 m and also the spectral bands were grouped in 3 different ways: RGB, IRG and the four channels altogether (figure 8). There were two runs with lidar variables: all of them altogether and using percentiles only. Lastly, the combined use of lidar variables and DMC data was analyzed. However, in all of the tests, the image segmentation was based only on the tree height.

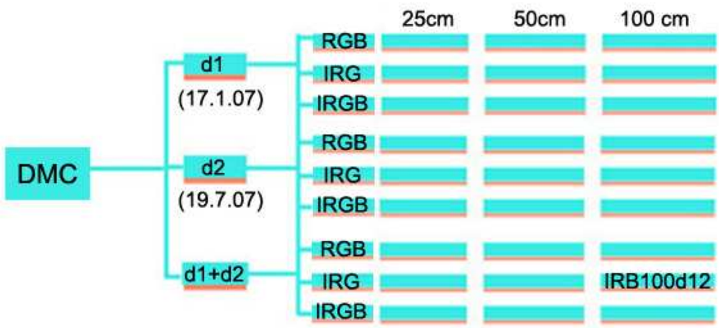

Figure 8. Classification trials performed from DMC data

For each eCognition project the classification steps were the following: Firstly, , all the segments were classified into three categories according the tree heigh variable: low vegetation (<26cm), trees (26cm to 10m) and high objects (>10m). The thresholds were chosen to reject grass, powerlines and high trees in forested areas. After that, and using the values of the variables selected in each trial for the training trees as a reference, all of the tree segments were classified as olive, almond or carob trees according to their values for the same variables, by nearest neighbour (figure 9). The performance of each classification was analyzed with a contingency table, where the classes assigned to the test set are compared to its true category.

Results

One eCognition trial was done only with lidar percentiles to analyze if they were useful to discriminating species. Percentiles are an attempt to catch the structural characteristics of the trees. In a first test the nine lidar-derived percentiles were considered and an optimization analysis was performed to detect what of them were the most explicative variables.. Results show that the more variables are employed, the better the discrimination between species but taking into account only the 3 best percentiles (p10, p15 and p35) the results were close to those obtained with all 9 parameters. However, according to the contingency tables, the classification results (Table 4) were poor, or even very poor for almond trees. Probably because almond trees had no leaves when lidar data was acquired and their structure could not be appropriately defined by percentiles.

	Olive	Carob	Almond	Total
Olive	79 (78)	16 (37)	28 (60)	123 (-)
Carob	5 (5)	26 (60)	5 (11)	36 (-)
Almond	17 (17)	1 (2)	14 (30)	32 (-)
Total	101 (-)	43 (-)	47 (-)	191 (62)

9 percentiles

	Olive	Carob	Almond	Total
Olive	78 (77)	14 (33)	27 (57)	119 (-)
Carob	5 (5)	24 (56)	1 (2)	30 (-)
Almond	18 (18)	5 (12)	19 (40)	42 (-)
Total	101 (-)	43 (-)	47 (-)	191 (63)

3-best percentiles (p10, p15 and p35)

Table 4 Contingency tables for percentiles data only (percentages into paretheses).

Taking into account all the 15 lidar derived parameters, the classification performance improved a lot, olive trees were correctly identified in 92% of the cases but for the other species the success rate was less than 70%. Discrimination between species reached its maximum when 10 variables were used. Rejected parameters in the optimization step were the percentiles p5, p75 and p90, the penetration coefficient and the coefficient of variation of the elevation (Table 5). Results were good enough for olive trees, however, for almond trees, results were poor.

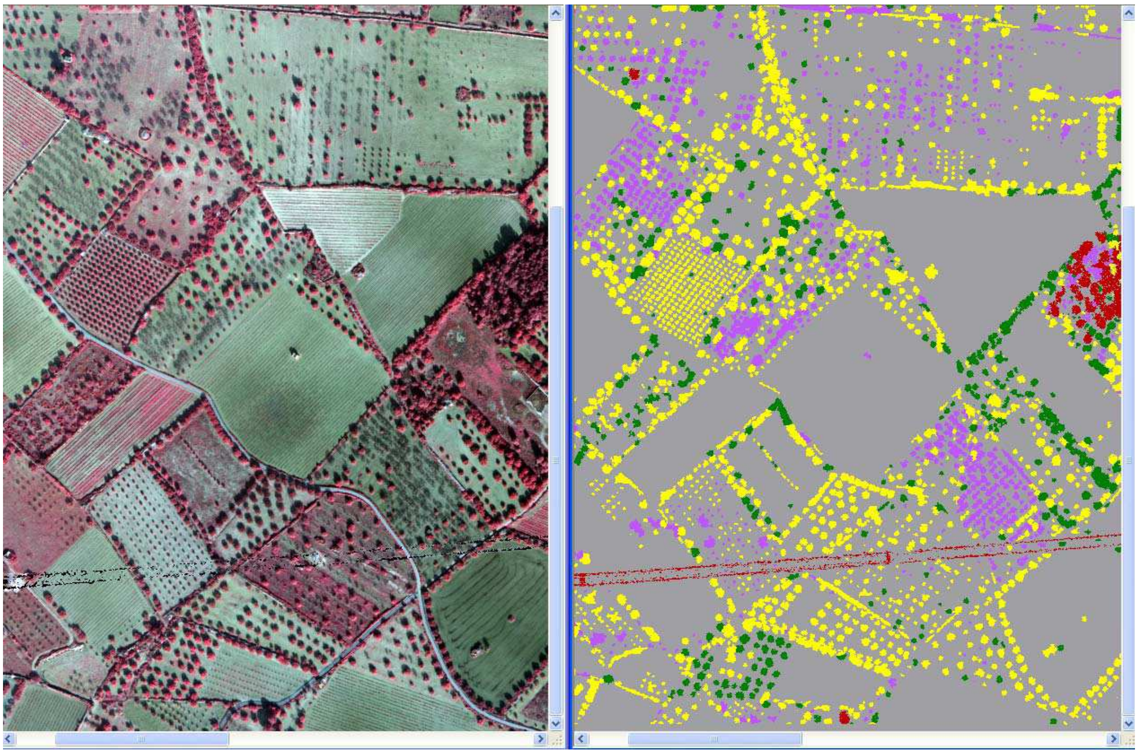

Figure 9. On the left, color infrared images. On the right, classification results corresponding to 100 cm resolution, multitemporal data and 4 spectral channels. Olives in yellow, carob in green, almond in purple, forest trees and powerlines in red, grass and ground in grey.

	Olive	Carob	Almond	Total
Olive	93 (92)	16 (37)	14 (30)	123 (-)
Carob	7 (7)	25 (58)	2 (4)	34 (-)
Almond	1 (1)	2 (5)	31 (66)	34 (-)
Total	101 (-)	43 (-)	47 (-)	191 (78)

15 lidar-derived parameters

	Olive	Carob	Almond	Total
Olive	90 (89)	16 (37)	14 (30)	120 (-)
Carob	8 (8)	25 (58)	1 (2)	34 (-)
Almond	3 (3)	2 (5)	32 (68)	37 (-)
Total	101 (-)	43 (-)	47 (-)	191 (77)

10-best lidar-derived parameters

Table 5 Contingency tables for lidar-derived parameters (percentages into paretheses).

The classification performance improved when multitemporal images from DMC were incorporated to the lidar data (10 lidar variables),, especially with the combination of infrared, green and red channels of each epoch (Table 6). The improvement is larger for carob (from 58% to 74%) and almond trees (from 68% to 98%) and smaller for olive trees (from 89% to 91%) because the good results achieved with lidar data in this case left little room for additional improvement.

	Olive	Carob	Almond	Total
Olive	92 (91)	11 (26)	1 (2)	104 (-)
Carob	9 (9)	32 (74)	0 (0)	41 (-)
Almond	0 (0)	0 (0)	46 (98)	46 (-)
Total	101 (-)	43 (-)	47 (-)	191 (89)

Table 6. Contingency table for the 10-best lidar-derived parameters plus I, R, G multitemporal channels of the DMC.

DMC data has also been analysed separately of lidar. In the following tests, only the lidar CHM image has been employed during the segmentation phase. Regarding the pixel size, no improvement was found using DMC images with 50 or 25 cm pixel size but this should not surprise us (Table 7). The reason is that virtual images of the DMC camera are a combination of 8 different images: a mosaic of 4 panchro images plus 4 spectral low resolution images (Hinz, 1999). All the CCDs have a pixel size of 12 μm but the lenses of the panchro cameras have a focal length of 120 mm and the spectral cameras have a focal length of 25 mm. Therefore, by construction, the resolution of the spectral channels is 4.8 times worse than the resolution of the panchromatic image. Resampling the virtual image to a pixel size of one meter has not reduced the original resolution of the spectral channels and, on the opposite, using highly pan-sharpened resolutions (25-50 cm) may degrade the spectral information.

Table 7. Multitemporal DMC data at different pixel sizes, 4 channels.

	Olive	Carob	Almond	Total
Olive	116 (91)	20 (38)	0 (0)	136
Carob	10 (8)	32 (60)	1 (2)	43
Almond	2 (2)	1 (2)	51 (98)	54
Total	128	53	52	233 (85)

25 cm

	Olive	Carob	Almond	Total
Olive	116 (94)	15 (29)	1 (2)	132
Carob	7 (6)	35 (69)	0 (0)	42
Almond	1 (1)	1 (2)	51 (98)	53
Total	124	51	52	227 (89)

50 cm

	Olive	Carob	Almond	Total
Olive	93 (92)	10 (23)	0 (0)	103
Carob	8 (8)	33 (77)	0 (0)	41
Almond	0 (0)	0 (0)	47 (100)	47
Total	101	43	47	191 (91)

100 cm

Infrared channel was decisive to detect carobs and the matching rate ranged from 60% without IR to 74% when IRC was used (table 8). However, blue channel is important to reduce confusion between olive trees from carobs in summer images (2nd epoch, table 8).

Table 8. Contingency tables for DMC visible channels (RGB) and IRC

	Olive	Carob	Almond	Total
Olive	78 (79)	17 (40)	1 (2)	96
Carob	18 (18)	24 (57)	0 (0)	42
Almond	3 (3)	1 (2)	46 (98)	50
Total	99	42	47	188 (79)

DMC 100 cm 1st epoch, RGB

	Olive	Carob	Almond	Total
Olive	85 (86)	13 (31)	0 (0)	98
Carob	14 (14)	29 (69)	0 (0)	43
Almond	0 (0)	0 (0)	47 (100)	47
Total	99	42	47	188 (86)

DMC 100 cm 1st epoch, IRC

	Olive	Carob	Almond	Total
Olive	92 (91)	18 (42)	3 (6)	113
Carob	7 (7)	18 (42)	6 (13)	31
Almond	2 (2)	7 (16)	38 (81)	47
Total	101	43	47	191 (77)

DMC 100 cm 2nd epoch, RGB

	Olive	Carob	Almond	Total
Olive	83 (82)	24 (57)	3 (6)	110
Carob	11 (11)	12 (29)	6 (13)	29
Almond	7 (7)	6 (14)	38 (81)	51
Total	101	42	47	190 (70)

DMC 100 cm 2nd epoch, IRC

	Olive	Carob	Almond	Total
Olive	89 (90)	15 (36)	2 (4)	106
Carob	8 (8)	25 (60)	0 (0)	33
Almond	2 (2)	2 (5)	45 (96)	49
Total	99	42	47	188 (85)

DMC 100 cm both epochs, RGB

	Olive	Carob	Almond	Total
Olive	94 (93)	11 (26)	0 (0)	105
Carob	7 (7)	32 (74)	0 (0)	39
Almond	0 (0)	0 (0)	47 (100)	47
Total	101	43	47	191 (91)

DMC 100 cm both epochs, IRC

Results from only one epoch were poorer for olive trees than those obtained from multitemporal images (tables 7 & 9) but winter images have been critical to discriminate almond trees.

Table 9. Contingency tables for DMC (all channels altogether)

	Olive	Carob	Almond	Total
Olive	83 (84)	9 (21)	0 (0)	92
Carob	16 (16)	33 (79)	0 (0)	49
Almond	0 (0)	0 (0)	47 (100)	47
Total	99	42	47	188 (87)

DMC 100 cm 1st epoch

	Olive	Carob	Almond	Total
Olive	85 (84)	18 (42)	5 (11)	108
Carob	7 (7)	21 (49)	5 (11)	33
Almond	9 (9)	4 (9)	37 (79)	50
Total	101	43	47	191 (75)

DMC 100 cm 2nd epoch

Conclusions

The height and crown area derived from lidar are in good agreement with field-measured values taking into account that the lidar point density that was employed in this study was low.

Taking into account the 15 lidar-derived parameters, olive trees were correctly identified in 92% of the cases but for the other species the success rate was less than 70%. The discrimination between species achieved a maximum with 10 variables, being p10, p15 and p35 the more interesting percentiles. With the employed parameters and point density, lidar was not enough to discriminate species but lidar results cannot be considered bad. There was an improvement on the rates for carob and almond trees when using the best 10 lidar variables plus multitemporal IRG data. The change for the olive trees was very small because they were well detected with lidar data alone. Anyway, the results with only DMC were similar or even better.

The lidar height has allowed individualizing the trees with high reliability probably because the trees were well isolated in the field. The combination of lidar with multispectral images has simplified the analysis avoiding confusion between trees and other covers with similar spectral response like grass or shrubs. Moreover, the tree segmentation allows concentrating the analysis on the crowns and to treat them as independent entities.

Regarding the geometric registering of the images, the lidar derived CHM has been decisive to rectify tree images from different epochs or different sensors keeping a correct overlap of the crowns. This rectification is necessary at high spatial resolutions.

Multitemporal images are required to properly discriminate the tree species and the epochs of each survey must be carefully chosen taking into account the species to be studied. Some dates are critical to obtain good results with some species.

Acknowlegment

This work would have not been possible without the dedication and helpful comments of many of our colleagues. We want to thank the help of Armand Güell, Wolfgang Kornus, Myriam Moysset, Ramon Alamús, Joan Martí, David Torrents, Jordi Hernández, Daniel Farré, José Antonio Ortega, Vicenç Palà, Anna Tardà, Fernando Pérez, Judit Fernández, Miquel Àngel Ortiz, Roman Arbiol, Julià Talaya and Xavier Esteve.

References

Chubey, M.S, Franklin S.E., and Wulder, M.A. Object-based analysis of Ikonos-2 imagery for extraction of forest inventory parameters, PERS, 2006; 72(4): 384-394.

Definiens AG, 2004. eCognition Version 4 User Guide.

Hinz, A. The Z/I digital aerial camera system. Proceedings of the 47th Photogrammetric Week. 1999, Stuttgart. Wichmann Verlag, Heidelberg, pp. 109-115.

Hyyppä, J. and Inkinen, M. Detecting and estimating attributes for single trees using laser scanner. Photogrammetric Journal of Finland, 1999; 16:27-42.

Holmgren, J. Estimation of forest variables using airborne laser scanning. Doctoral dissertation. Dept. of Forest Resource Management and Geomatics, SLU. Acta Universitatis agriculturae Sueciae. Silvestria, 2003; 278, 43pp.

Kornus W. and Ruiz A. Strip Adjustment of LIDAR Data. ISPRS Workshop on Airborne Laserscanning, "3-D reconstruction from airborne laserscanner and InSAR data", 8-10 October, 2003. Dresden.

Lee. J.-H., and Joshua B. Fisher. ASPRS Annual Conference. 1-5 May, 2006. Reno, Nevada.

Naesset, E. and Bjerknes, K.O. Estimating tree heights and number of stems in young forest stands using airborne laser scanner data. Remote Sensing of Environment 2001;78, 328-340.

Palà, V., Arbiol, R., Pérez, F. Generación de ortoimágenes en áreas urbanas. Revista de Teledetección, 2001; 16: 47-50.

Palà, V., Arbiol, R. True orthoimage generation in urban areas. Proc. of the 3rd International Symposium Remote Sensing of Urban Areas. Istambul, 2002; 1: 309-314.

Popescu, S.C., and Randolph H. Wynne. Seeing the trees in the forest: using lidar and multispectral data fusion with local filtering and variable window size for estimating tree height. PERS 2004; 70:589-604.

Viau, A.A, Jang, J.-D., Payan, V. and A. Devost. The use of airborne Lidar ans multispectral sensors for orchard tree inventory and characterization. 7 th Fruit, Nut and Vegetable Production Engineering Symposium “FRUTIC 05”, Montpellier, 2005. pag. 689-698.

Viñas, O., Ruiz, A., Xandri, R., Palà, V., Arbiol, R. Combined use of Lidar and Quickbird data for the generation of land use maps ISPRS Mid-term Sysposium “From Pixels to Processes”. Enschede, 8-11 May, 2006.